Assessment of layerwise user-elements in Abaqus for static and free vibration analysis of variable stiffness composite laminates

Composite Structures 303 (2023) 116291

Contents lists available at ScienceDirect

Composite Structures

journal homepage: www.elsevier.com/locate/compstruct

Assessment of layerwise user-elements in Abaqus for static and free vibration analysis of variable stiffness composite laminates

J.A. Moreira [a,*], F. Moleiro [a], A.L. Araújo [a], A. Pagani [b]

[a] IDMEC, Instituto Superior Tecnico, Universidade de Lisboa, Av. Rovisco Pais 1, Lisboa, 1049-001, Portugal
[b] MUL2, Department of Mechanical and Aerospace Engineering, Politecnico di Torino, Corso Duca degli Abruzzi 24, Torino, 10129, Italy

ARTICLE INFO

Keywords:
Abaqus user-elements
Variable stiffness composites
Curvilinear fibre paths
Layerwise theory
Shear deformation theories

ABSTRACT

In this work, user-elements (UEL) in Abaqus are taken a step forward into the high-order layerwise modelling of variable stiffness composite laminates with curvilinear fibre paths, extending the limited number of available literature on refined multilayered UEL models. Two layerwise UEL models with three discrete layers are here proposed, assigning to each layer the displacements of the first- and third-order shear deformation theories, thus named UEL1 and UEL3, respectively. A complete assessment of the models predictive capabilities is carried out by a comparison with available static and free vibration solutions in the literature – either for constant or variable stiffness laminates – considering various boundary and loading conditions, as well as thin and moderately thick plates. Numerical results demonstrate that the developed models are capable to render fairly accurate and computationally efficient results, with particular emphasis on the higher-order model for predicting the global–local response behaviour of moderately thick plates.

1. Introduction

The ever-growing advances in composite material science have provided crucial achievements in the design technology of lightweight and high strength structures for various cutting-edge engineering applications. In particular, the recent advances in automated manufacturing techniques [1,2] shed light on the capability of tailoring variable stiffness composites (VSC), with curvilinear fibre paths, as an emerging and promising structural technology to further improve the performance of the conventional constant stiffness composite (CSC) laminates with straight fibres. Therefore, it is crucial the development of refined finite element (FE) models suitable for an accurate design and analysis of curvilinear fibre composite laminates. In response to the limited number of available literature on refined multilayered models implemented through the user-element (UEL) subroutine in Abaqus, this work focuses on the development and assessment of two layerwise (LW) user-elements for static and free vibration analysis of VSC laminates, including high-order modelling for the first time available. Thus, pushing forward the current knowledge on the application of UEL models to render numerically accurate and computationally efficient analyses of advanced composite laminates within a standard and broadly used commercial software.

Since the leading works by Gürdal and Olmedo [3,4], in the early 1990s, on the in-plane and buckling response of VSC laminates with spatially varying fibre orientations – also called variable angle-tow (VAT) laminates – the VSC design technology have received a tremendous research interest. Actually, the exceptional tailor-ability of VSC laminates relies mostly on a broad design space of fibre orientations throughout the lamination scheme, turning them suitable to be optimized for various operational conditions. Hence, despite the original purpose of using VSCs to improve buckling stability, more applications have been addressed, including the maximization of the fundamental frequency [5], the optimization of buckling and first-ply failure responses [6], the minimization of maximum deflections [7] or even the aeroelastic stability augmentation [8,9] (just to name a few noteworthy works).

In view of the assessment of finite element (FE) models based on High-Order Shear Deformation Theories (HSDT) for the analysis of VSC laminated plates, Akhavan and Ribeiro [10] and Akhavan et al. [11] applied the Reddy's Third-Order Shear Deformation Theory (TSDT) for free vibration analysis and evaluation of large deflections and stresses, respectively. It is emphasized that the Reddy's TSDT is based on an Equivalent Single Layer (ESL) description and therefore, Yazdani et al. [12] as well as Yazdani and Ribeiro [13,14] developed a *p*-version LW model assigning the First-Order Shear Deformation Theories (FSDT) displacement field for each composite layer.

Moreover, regarding the application of more advanced and unified frameworks, such as the Generalized Unified Formulation (GUF), Demasi et al. [15] reported some numerical assessments on the linear

* Corresponding author.
E-mail address: joao.anjos.moreira@tecnico.ulisboa.pt (J.A. Moreira).

https://doi.org/10.1016/j.compstruct.2022.116291
Received 3 April 2022; Received in revised form 22 September 2022; Accepted 29 September 2022
Available online 4 October 2022

static analysis of VSC plates, employing ESL and LW descriptions, with various orders of expansion for each displacement variable. As far as VSC laminated shells are concerned, Tornabene et al. [16] introduced the Carrera Unified Formulation (CUF) for static analysis of doubly-curved VSC laminates and Sánchez-Majano et al. [17] focused on the accuracy assessment of LW and ESL descriptions in stress analysis of VSC shells. Besides the previously mentioned studies on static response, the free vibration analysis of VSC laminates through refined 1D CUF elements was firstly presented by Viglietti et al. [18,19] and further extended by Yan et al. [20]. An additional remark may be noteworthy concerning the recent works by Pagani and Sánchez-Majano [21,22] devoted to the influence analysis of manufacturing defects on the buckling behaviour and failure onset of VSC laminates, applying once again the CUF.

Concerning the computational implementation of FE models, the approach typically followed by researchers is the development of in-house programmes (for instance in Matlab or Fortran environment). However, it is possible to define customizable user-elements in some commercial finite element codes, such as the broadly used Abaqus. For doing so, Abaqus provides the UEL subroutine, where the definitions associated with a certain FE formulation are translated into a straightforward Fortran code, linked to the main software. Thus, the user can take advantage of the native pre- and post-processing features, as well as the different solvers. In fact, even thought Ferreira et al. [23] have discussed the implementation of a user-element based on the CUF, the paper was limited to ESL descriptions applied to stress analysis. Therefore, Moreira et al. [24] addressed the implementation of LW electro-elastic user-elements for the static and free vibration analysis of piezoelectric composite plates. For three discrete layers, the electro-elastic UEL models assume a piecewise continuous FSDT displacement field, combined with a linear or quadratic through-thickness distribution of the electric potential.

In the present work, LW user-elements in Abaqus are taken a step forward to the analysis of VSC laminates with curvilinear fibre paths, including both first- and high-order models. To the best of the authors' knowledge, this is the first time that a high-order LW element is implemented through the UEL subroutine, being also among the few available works that apply and compare LW descriptions for both static and free vibration analysis of VSC laminates. Two LW user-element models with three discrete layers are here proposed, assigning to each layer continuous through-thickness distributions of displacements using the first- and third-order shear deformation theories, thus named UEL1 and UEL3, respectively.

Numerical applications consider the static and free vibration analysis of both straight and curvilinear fibre composite laminates, i.e. CSC and VSC laminates, respectively, assuming various boundary and loading conditions, as well as two side-to-thickness ratios to address both thin and moderately thick plates. The accuracy assessment of the UEL models is firstly provided by a comparison with three-dimensional (3D) exact static and free vibration solutions for simply supported CSC laminates developed by Moleiro et al. [25]. Then, regarding the analysis of VSC laminates, the present models predictive capabilities are compared with available FE solutions in the literature, namely Marques et al. [7] in static analysis of maximum deflections, as well as Akhavan and Ribeiro [10] and Viglietti et al. [18] in free vibration analysis. The test cases consist of three VSC laminates with linear fibre angle distributions. Nevertheless, a conventional cross-ply laminate is also considered throughout the analyses to further compare the VSC laminates with a quite standard CSC laminate, including the through-thickness distribution of displacements and stresses as well.

2. Layerwise models

In the present work, two LW models involving three discrete layers – top (t), core (c) and bottom (b), as schematically represented in Fig. 1 – are implemented using the UEL subroutine in Abaqus. For each discrete layer, the developed UEL1 and UEL3 models assign the displacement field of the FSDT and TSDT, respectively.

The layers are assumed to be perfectly bonded to each other, being made of a purely elastic composite material with orthotropic symmetry and in-plane continuous graded properties introduced by spatially varying fibre orientations (i.e. curvilinear fibre paths). Hence, for each material layer, the plane stress constitutive equations, written in the global coordinate system (x, y, z), are given as shown:

$$\begin{Bmatrix} \sigma_{xx} \\ \sigma_{yy} \\ \sigma_{yz} \\ \sigma_{xz} \\ \sigma_{xy} \end{Bmatrix} = \begin{bmatrix} \bar{Q}_{11} & \bar{Q}_{12} & 0 & 0 & \bar{Q}_{16} \\ \bar{Q}_{12} & \bar{Q}_{22} & 0 & 0 & \bar{Q}_{26} \\ 0 & 0 & \bar{Q}_{44} & \bar{Q}_{45} & 0 \\ 0 & 0 & \bar{Q}_{45} & \bar{Q}_{55} & 0 \\ \bar{Q}_{16} & \bar{Q}_{26} & 0 & 0 & \bar{Q}_{66} \end{bmatrix} \begin{Bmatrix} \epsilon_{xx} \\ \epsilon_{yy} \\ \gamma_{yz} \\ \gamma_{xz} \\ \gamma_{xy} \end{Bmatrix} \tag{1}$$

where σ_{ij} denotes the stress tensor components, while ϵ_{ii} and γ_{ij} are the infinitesimal normal strains and the engineering shear strains, respectively. The reduced elastic constants $\bar{Q}_{ij}$ are given explicitly in Reddy [26] resorting to the well-known rotation matrix between the material axes of orthotropy and the global coordinate system.

For conciseness, Eq. (1) is written in the following compact form:

$$\{\sigma\} = \left[\bar{Q}\right] \{\varepsilon\} \tag{2a}$$

Additionally, since only small displacements are considered, the linear strain–displacement relation is given by:

$$\epsilon_{ij} = \frac{1}{2}\left(u_{i,j} + u_{j,i}\right) \tag{3}$$

where $(u_1, u_2, u_3) \equiv (u, v, w)$ are the displacement components in the x-, y- and z-axis, respectively, and the comma-derivative notation is here adopted. The engineering shear strains are given by $\gamma_{ij} = 2\epsilon_{ij}$.

Within the scope of this work, the variable stiffness composites herein modelled are fibre reinforced composites with curvilinear fibre paths, where a reference path is shifted along an axis to create the remaining paths, lying at a fixed distance between each other. One of the crucial aspects related to the modelling of curvilinear fibre composites is the parametrization of the fibre trajectories, which are supposed to be continuous curvilinear paths, with a reduced number of parameters suitable to completely define the overall orientations. Hence, the local fibre angle is a function of the in-plane coordinates, i.e. $\theta(x, y)$, and therefore the reduced elastic constants in the global coordinate system are in-plane continuously graded $\bar{Q}_{ij}(x, y)$ as well.

In line with the leading works by Gürdal and Olmedo [3,4], a linear fibre angle distribution along the x-axis, with two control angles, is considered in the present paper. Regardless of manufacturing limitations on the maximum curvature that can be introduced into a fibre path, which shorten the feasible design space of control angles $\langle T_0, T_1 \rangle$, the fibre angle distribution is given as follows:

$$\theta(x) = T_0 + \frac{2(T_1 - T_0)}{a}\left|x - \frac{a}{2}\right| \tag{4}$$

where $T_0 = \theta(a/2)$ and $T_1 = \theta(0) = \theta(a)$ are the fibre orientations at the centre and edges of the plate, respectively, as illustrated in Fig. 2.

The through-thickness distribution of the LW displacement field, assigned by each UEL model, is presented in the following subsections. Nevertheless, for the three discrete layers, the interlaminar continuity conditions of each i-displacement component are given as shown:

$$u_i^c\left(x, y, z = h_c/2\right) = u_i^t\left(x, y, z = \bar{z}_t - h_t/2\right) \tag{5a}$$

$$u_i^c\left(x, y, z = -h_c/2\right) = u_i^b\left(x, y, z = \bar{z}_b + h_b/2\right) \tag{5b}$$

where h_k is the k-layer thickness and, as shown in Fig. 1, $\bar{z}_t$ and $\bar{z}_b$ are the mid-plane transverse coordinates of the top and bottom layers, respectively.

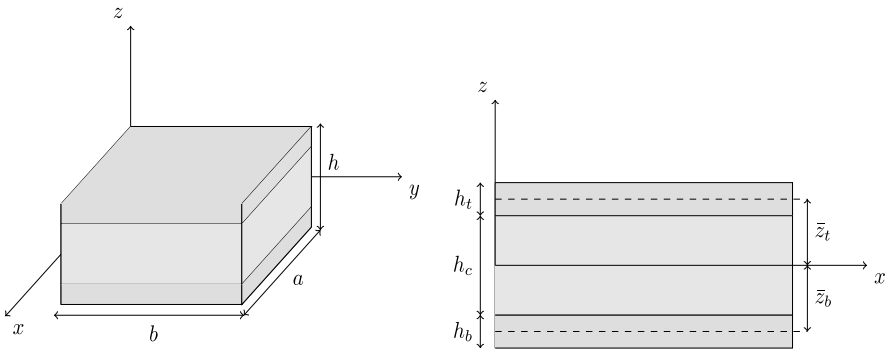

Fig. 1. Laminated composite plate divided in three discrete layers: top, core and bottom.

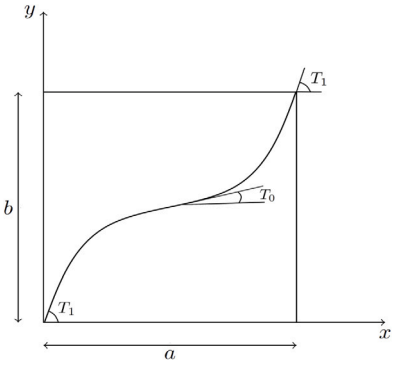

Fig. 2. Curvilinear fibre composite layer with a linear fibre angle distribution along the x-axis.

2.1. First-order shear deformation model

The displacement field of the UEL1 model is derived upon the application of the FSDT [26] to each discrete layer, fulfilling *a priori* the interlaminar continuity conditions given in Eq. (5). Thus, the continuity of displacements is ensured at the interfaces between adjacent layers, while reducing the total number of independent variables needed to address the through-thickness distribution of the displacement field.

In line with Moreira et al. [24], the LW FSDT displacement field of the three discrete layers is given as shown:

$$u^c(x,y,z) = u_0^c(x,y) + z\theta_x^c(x,y) \tag{6a}$$

$$v^c(x,y,z) = v_0^c(x,y) + z\theta_y^c(x,y) \tag{6b}$$

$$u^t(x,y,z) = u_0^t(x,y) + (z-\bar{z}_t)\left(\alpha_1 u_0^c(x,y) + \alpha_2\theta_x^c(x,y) + \alpha_3 u_0^t(x,y)\right) \tag{6c}$$

$$v^t(x,y,z) = v_0^t(x,y) + (z-\bar{z}_t)\left(\alpha_1 v_0^c(x,y) + \alpha_2\theta_y^c(x,y) + \alpha_3 v_0^t(x,y)\right) \tag{6d}$$

$$u^b(x,y,z) = u_0^b(x,y) + (z-\bar{z}_b)\left(\beta_1 u_0^c(x,y) + \beta_2\theta_x^c(x,y) + \beta_3 u_0^b(x,y)\right) \tag{6e}$$

$$v^b(x,y,z) = v_0^b(x,y) + (z-\bar{z}_b)\left(\beta_1 v_0^c(x,y) + \beta_2\theta_y^c(x,y) + \beta_3 v_0^b(x,y)\right) \tag{6f}$$

$$w^c(x,y,z) = w^t(x,y,z) = w^b(x,y,z) = w_0(x,y) \tag{6g}$$

where the subscript 0 stands for the mid-plane location of the layer, while θ_x^c and θ_y^c denote the rotations of the normals to the mid-plane about the y- and x-axes of the core, respectively.

As derived from the interlaminar continuity conditions, the layerwise-constants α_j and β_j, with $j = \{1,2,3\}$, are given by:

$$\alpha_1 = -2/h_t,\ \alpha_2 = -h_c/h_t,\ \alpha_3 = -\alpha_1 \tag{7a}$$

$$\beta_1 = 2/h_b,\ \beta_2 = -h_c/h_b,\ \beta_3 = -\beta_1 \tag{7b}$$

Overall, the displacement vector $\{u\}^k$ of each k-layer, with $k = \{t,c,b\}$, is related to the mechanical degrees of freedom (DOFs) vector $\{d_1\}$, i.e. the nine independent mechanical unknowns associated to the LW FSDT displacements in Eq. (6), by a 3×9 matrix $[Z_1]_k$, which allows the following relation:

$$\{u\}^k = \left\{u^k\ v^k\ w^k\right\}^T = [Z_1]_k\{d_1\} \tag{8a}$$

$$\{d_1\} = \left\{u_0^c\ v_0^c\ w_0\ \theta_x^c\ \theta_y^c\ u_0^t\ v_0^t\ u_0^b\ v_0^b\right\}^T \tag{8b}$$

In view of Eqs. (1), (3) and (6), one obtains that the FSDT based model (UEL1) predicts a linear through-thickness distribution of in-plane stresses in each material layer, along with just constant transverse shear stresses.

2.2. Third-order shear deformation model

The third-order shear deformation model, implemented as UEL3, considers a TSDT displacement field within each discrete layer. In particular, the TSDT assumes a cubic z-expansion of in-plane displacements and keeps the transverse inextensibility as the FSDT (i.e. $\varepsilon_{zz} = 0$). Imposing the interlaminar continuity conditions given in Eq. (5), one can derive the following LW TSDT displacement field:

$$u^c(x,y,z) = u_0^c(x,y) + z\theta_x^c(x,y) + z^2\varkappa_x^c(x,y) + z^3\lambda_x^c(x,y) \tag{9a}$$

$$v^c(x,y,z) = v_0^c(x,y) + z\theta_y^c(x,y) + z^2\varkappa_y^c(x,y) + z^3\lambda_y^c(x,y) \tag{9b}$$

$$\begin{aligned} u^t(x,y,z) = {} & \alpha_1 u_0^c(x,y) + \alpha_2\theta_x^c(x,y) + \alpha_3\varkappa_x^c(x,y) + \alpha_4\lambda_x^c(x,y) + \alpha_5\theta_x^t(x,y) + \\ & \alpha_6\varkappa_x^t(x,y) + \alpha_7\lambda_x^t(x,y) + (z-\bar{z}_t)\theta_x^t(x,y) + (z-\bar{z}_t)^2\varkappa_x^t(x,y) + \\ & (z-\bar{z}_t)^3\lambda_x^t(x,y) \end{aligned} \tag{9c}$$

$$\begin{aligned} v^t(x,y,z) = {} & \alpha_1 v_0^c(x,y) + \alpha_2\theta_y^c(x,y) + \alpha_3\varkappa_y^c(x,y) + \alpha_4\lambda_y^c(x,y) + \alpha_5\theta_y^t(x,y) + \\ & \alpha_6\varkappa_y^t(x,y) + \alpha_7\lambda_y^t(x,y) + (z-\bar{z}_t)\theta_y^t(x,y) + (z-\bar{z}_t)^2\varkappa_y^t(x,y) + \\ & (z-\bar{z}_t)^3\lambda_y^t(x,y) \end{aligned} \tag{9d}$$

$$\begin{aligned} u^b(x,y,z) = {} & \beta_1 u_0^c(x,y) + \beta_2\theta_x^c(x,y) + \beta_3\varkappa_x^c(x,y) + \beta_4\lambda_x^c(x,y) + \beta_5\theta_x^b(x,y) + \\ & \beta_6\varkappa_x^b(x,y) + \beta_7\lambda_x^b(x,y) + (z-\bar{z}_b)\theta_x^b(x,y) + (z-\bar{z}_b)^2\varkappa_x^b(x,y) + \\ & (z-\bar{z}_b)^3\lambda_x^b(x,y) \end{aligned} \tag{9e}$$

$$\begin{aligned} v^b(x,y,z) = {} & \beta_1 v_0^c(x,y) + \beta_2\theta_y^c(x,y) + \beta_3\varkappa_y^c(x,y) + \beta_4\lambda_y^c(x,y) + \beta_5\theta_y^b(x,y) + \\ & \beta_6\varkappa_y^b(x,y) + \beta_7\lambda_y^b(x,y) + (z-\bar{z}_b)\theta_y^b(x,y) + (z-\bar{z}_b)^2\varkappa_y^b(x,y) + \\ & (z-\bar{z}_b)^3\lambda_y^b(x,y) \end{aligned} \tag{9f}$$

$$w^c(x,y,z) = w^t(x,y,z) = w^b(x,y,z) = w_0(x,y) \tag{9g}$$

where $(\varkappa_x^k, \varkappa_y^k)$ and $(\lambda_x^k, \lambda_y^k)$ are the higher-order generalized displacements of each k-layer.

The associated layerwise-constants α_j and β_j, with $j = \{1,\ldots,7\}$, are given by:

$$\alpha_1 = 1,\ \alpha_2 = h_c/2,\ \alpha_3 = \alpha_2^2,\ \alpha_4 = \alpha_2^3,\ \alpha_5 = h_t/2,\ \alpha_6 = -\alpha_5^2,\ \alpha_7 = \alpha_5^3 \tag{10a}$$

$$\beta_1 = 1,\ \beta_2 = -h_c/2,\ \beta_3 = \beta_2^2,\ \beta 4 = -\beta_2^3,\ \beta_5 = -h_b/2,\ \beta_6 = -\beta_5^2,\ \beta_7 = \beta_5^3 \tag{10b}$$

In the LW TSDT model, the in-plane displacements of the top and bottom layers mid-plane are written as a linear combination of the remaining generalized displacements of the model. Therefore, one obtains finite layerwise-constants when setting a null thickness for the top and bottom layers in Eq. (10), using then the middle discrete layer as an ESL representative of the whole laminate.

To summarize, the displacement vector of each k-layer, with $k = \{t, c, b\}$, is obtained from the DOFs vector $\{d_3\}$, i.e. the twenty one independent generalized displacements associated to the LW displacements in Eq. (9), defining a 3×21 matrix, denoted by $[Z_3]_k$, which allows the following relation:

$$\{u\}^k = \left\{u^k\ v^k\ w^k\right\}^T = [Z_3]_k\{d_3\} \tag{11a}$$

$$\{d_3\} = \left\{u_0^c\ v_0^c\ w_0\ \theta_x^c\ \theta_y^c\ \varkappa_x^c\ \varkappa_y^c\ \lambda_x^c\ \lambda_y^c\ \theta_x^t\ \theta_y^t \times\ \varkappa_x^t\ \varkappa_y^t\ \lambda_x^t\ \lambda_y^t\ \theta_x^b\ \theta_y^b\ \varkappa_x^b\ \varkappa_y^b\ \lambda_x^b\ \lambda_y^b\right\}^T \tag{11b}$$

It is emphasized that for FSDT based model, a similar nomenclature was adopted in Eq. (8), but using an index '1' instead of '3' in light of the piecewise linear theory.

Moreover, according to Eqs. (1), (3) and (9), one concludes that the TSDT based model (UEL3) predicts a cubic through-thickness distribution of in-plane stresses in each material layer, along with quadratic transverse shear stresses. Actually, the parabolic profile of transverse shear strains, instead of the just constant in the FSDT, does not requires the application of a shear correction factor and allows a closer fulfilment of the stress-free boundary conditions, i.e. null transverse shear stresses on the upper and lower surfaces of the laminate, as well as of the interlaminar continuity conditions of transverse shear stresses.

3. Finite element formulation

For both FSDT and TSDT based formulations used in the UEL1 and UEL3, respectively, the FE approximations in-plane are achieved using eight-node quadratic serendipity interpolation functions [26] for the DOFs in Eqs. (8b) and (11b). For brevity, since the FE formulation of the models is similar, it is present in a general fashion, omitting systematically the index associated to the model. Hence, for each model, a general matrix form of the FE approximations of the elements DOFs $\{d\}^{(e)}$ can be written as shown:

$$\{d\}^{(e)} = [N]\{\Delta\}^{(e)},\quad \{\Delta\}^{(e)} = \{\{d\}_1^{(e)^T} \ldots \{d\}_8^{(e)^T}\}^T \tag{12}$$

where the matrix $[N]$ contains the interpolation functions in eight $n_d \times n_d$ diagonal blocks, where n_d is the number of DOFs per node of the model (i.e. 9 and 21 for the UEL1 and UEL3, respectively).

Additionally, for each k-layer, with $k = \{t, c, b\}$, the relation between the strain vector and the nodal DOFs is given by:

$$\{\varepsilon\}_k = [S]_k[B]_k\{\Delta\} \tag{13}$$

where the transverse functions are featured in the $[S]_k$ matrices, while the in-plane interpolation functions and their derivatives are isolated within the $[B]_k$ matrices. The entries and dimensions of these matrices are dependent on the UEL model.

The dynamic equilibrium equations of the elements are derived applying the Hamilton's principle [24], the constitutive law in Eq. (2), the displacement-DOFs relation in Eq. (12) and the strain-DOFs relation in Eq. (13), leading to the usual canonical form as follows:

$$\left[M\right]^{(e)}\{\ddot{\Delta}\} + \left[K\right]^{(e)}\{\Delta\} = \{F\}^{(e)} \tag{14}$$

where $\{\ddot{\Delta}\}$ and $\{\Delta\}$ are the nodal DOFs and their second time derivatives, respectively.

Moreover, $\left[M\right]^{(e)}$ and $\left[K\right]^{(e)}$ are the element mass and stiffness matrices, respectively, while $\{F\}^{(e)}$ is element force vector, which are all together given by:

$$\left[M\right]^{(e)} = \sum_{k=c,t,b}\int_{-1}^{1}\int_{-1}^{1}\rho_k\,[N]^T\,[P]_k\,[N]\,\mathcal{J}\,d\xi d\eta \tag{15a}$$

$$\left[K\right]^{(e)} = \sum_{k=c,t,b}\int_{-1}^{1}\int_{-1}^{1}[B]_k^T\,[\hat{Q}]_k\,[B]_k\,\mathcal{J}\,d\xi d\eta \tag{15b}$$

$$\{F\}^{(e)} = \sum_{k=c,t,b}\int_{-1}^{1}\int_{-1}^{1}[N]^T\,[Z]_k^T\,\left\{f_s\right\}_k\,\mathcal{J}\,d\xi d\eta \tag{15c}$$

where ρ_k and $\left\{f_s\right\}_k$ denote the density and the surface forces of each k-layer, respectively, while $\mathcal{J}$ is the determinant of the Jacobian needed to numerically evaluate the integrals by Gauss quadrature in natural coordinates (ξ, η). In addition, for the FSDT based model (UEL1), a shear correction factor of a unit value is adopted, as suggested by Birman and Bert [27] for sandwich plates (being indeed the assumed value by Moreira et al. [24] as well).

Furthermore, the $[P]_k$ matrix in Eq. (15a), as well as the generalized elastic matrix $[\hat{Q}]_k$ in Eq. (15b), are obtained following the analytical integration on the transverse direction of each discrete layer as shown:

$$[P]_k = \int_{z_k^i}^{z_k^s}[Z]_k^T\,[Z]_k\,dz \tag{16a}$$

$$[\hat{Q}]_k = \int_{z_k^i}^{z_k^s}[S]_k^T\,\left[\bar{Q}\right]_k\,[S]_k\,dz \tag{16b}$$

where z_k^i and z_k^s, with $k = \{c, t, b\}$, are the k-layer z-coordinates of the lower and upper surfaces, respectively. For laminates with more than three layers, a subdivision in three sublaminates must be carried out, each one treated as a sole ESL. Thus, for each k-layer that mathematically represents a sublaminate, the thickness integration of the reduced elastic constants in Eq. (16b) is indeed the sum of the integrals on the transverse direction of each material layer within the sublaminate.

It is worth remarking that an accurate discretization of the in-plane distributed stiffness introduced by curvilinear fibre composites, which relies mostly on a low discretization error of the fibre angle distribution, is ensured through the evaluation of the fibre orientations in each integration point. Therefore, when sufficiently refined meshes are applied, a quasi-continuous description of the fibre angle distribution in-plane is achieved. For doing so, the transformation between the natural coordinates (ξ, η) and the global coordinates (x, y) is applied to obtain the integration points within an element, written in the global axes [26]. Then, for each integration point, the local fibre angle is assessed for a predetermined fibre angle distribution, underlying the final evaluation of the local reduced elastic constants in Eq. (1).

4. Abaqus user-element implementation

The UEL subroutine is an advanced tool provided by the commercial software Abaqus, where users can implement their own FE models to be applied in a large number of analyses. The subroutine is coded in Fortran, using a default heading (provided in [23]) to get the interaction with Abaqus. For each user-element within a mesh, Abaqus calls the subroutine to evaluate the necessary element matrices, which are typically coded through loops on the integration points, including the right-hand side vector if necessary.

For static analysis, even though the inertial terms in Eq. (14) are neglected, the mass matrix is defined within the UEL subroutine as an identity matrix, with the same dimension as the stiffness matrix. In addition, the element stiffness matrix, given in Eq. (15b) is obtained using Gauss numerical integration, with reduced integration for the shear terms to avoid shear locking [26]. Actually, for the case of VSC laminates, it is emphasized that the integration of the membrane, bending and coupling membrane-bending stiffness terms is not fully

exact. Nevertheless, following the local fibre orientation modelling methodology previously explained, the fibre angle in each integration point is assessed and the elastic constants are updated accordingly (thus promoting an accurate evaluation of the distributed stiffness when refined meshes are applied). Moreover, as followed by Moreira et al. [24], the post-processing of stresses is performed at the integration points, using then direct local extrapolation.

Furthermore, when free vibration analysis is considered, the computation of the mass matrix, provided in Eq. (15a), is also numerically performed using Gauss integration. Additionally, no external forces are applied on the structure and the element DOFs are supposed to be harmonic.

For each laminated plate, an UEL subroutine must be written and a fibre angle distribution prescribed if necessary. Hence, for different fibre angle distributions, a given UEL subroutine is coded, changing solely the $\theta(x, y)$ function. Besides the subroutine (*.for* extension), a text file defining the intended analysis, known as the input file (*.inp* extension), must be provided as well.

Further details on the implementation of Abaqus user-elements are presented by Moreira et al. [24], explaining precisely the nomenclature, flowchart, input and output variables, as well as the application of boundary and loading conditions. A template input file is also provided, including the definition of a dummy mesh, which is used to: (i) apply transverse forces without programming the force vector and (ii) visualize the nodal variables within Abaqus/Viewer. Actually, the distributed surface loads are defined using the DLOAD subroutine. It is worth remarking that in present work, the nine active DOFs of the UEL1, stated in Eq. (8), are numbered in the input file as 1–6 and 14–16, while the UEL2 ones, defined in Eq. (11), are ordered as 1–6 and 14–28.

5. Numerical applications

As intended by this work, to verify the formulation and implementation of the proposed models, numerical applications consider the static and free vibration analysis of both straight and curvilinear fibre composite laminated plates. The accuracy assessment is carried out for various boundary and loading conditions, including the case of thin and moderately thick plates to further compare the UEL models.

As a first validation of the developed UEL models, the static and free vibration analysis of a simply-supported CSC laminate (0/90/0) is presented and compared with 3D exact solutions reported by Moleiro et al. [25]. Accordingly, the static response is evaluated for plates with the upper surface subjected to bi-sinusoidal transverse load given by:

$$q(x, y) = q_0 \sin(\pi x/a) \sin(\pi y/a) \tag{17}$$

In line with the original benchmark by Pagano [28], as also followed by Moleiro et al. [25], it is assumed square plates ($a = b$) with two side-to-thickness ratios, viz. $a/h = 100$ and 10, to assess the case of thin and moderately thick plates, respectively. The composite layers have an equal thickness $h/3$ and the following material properties: $E_1 = 25E_0$, $E_2 = E_3 = E_0$, $G_{12} = G_{13} = 0.5E_0$, $G_{23} = 0.2E_0$, $\nu_{12} = \nu_{13} = \nu_{23} = 0.25$ and $\rho = 1600$ kg/m^3, with $E_0 = 7$ GPa.

All results are given using the following nondimensionalized form:

$$\begin{aligned}
&[\tilde{u}, \tilde{v}] = \frac{100E_0h^2}{q_0a^3}[u, v], \quad \tilde{w} = \frac{100E_0h^3}{q_0a^4}w \\
&[\tilde{\sigma}_{xx}, \tilde{\sigma}_{yy}, \tilde{\sigma}_{xy}] = \frac{h^2}{q_0a^2}[\sigma_{xx}, \sigma_{yy}, \sigma_{xy}] \\
&[\tilde{\sigma}_{xz}, \tilde{\sigma}_{yz}] = \frac{h}{q_0a}[\sigma_{xz}, \sigma_{yz}]
\end{aligned} \tag{18}$$

where E_0 has the aforementioned value and q_0 is the amplitude value of the transverse load.

Regarding VSC laminates, three symmetric laminates are investigated, having each layer a linear fibre angle distribution along the x-axis as given in Eq. (4). A cross-ply CSC laminate is also considered throughout all analyses to compare the response behaviour of the VSC laminates with a conventional composite laminate. The stacking sequences are the following:

- *Constant stiffness composite (CSC)*: (0/90/0)
- *Variable stiffness composite 1 (VSC1)*: $(\langle 0, 45\rangle/\langle -45, -60\rangle/\langle 0, 45\rangle)$
- *Variable stiffness composite 2 (VSC2)*: $(\langle 30, 0\rangle/\langle 45, 90\rangle/\langle 30, 0\rangle)$
- *Variable stiffness composite 3 (VSC3)*: $(\langle 90, 45\rangle/\langle 60, 30\rangle/\langle 90, 45\rangle)$

For the accuracy assessment of the developed UEL models in the analysis of VSC laminates, numerical results are compared with FE solutions available in the literature, namely Marques et al. [7] for static analysis, as well as Akhavan and Ribeiro [10] and Viglietti et al. [18] for free vibration analysis. Hence, to be consistent with the benchmarks, the square plates have a fixed side $a = b = 1$ m and a total thickness h determined by the side-to-thickness ratio $a/h = 100$ and 10, i.e. thin and moderately thick plates, respectively. The material properties of the (equal thickness) composite layers are the following: $E_1 = 173$ GPa, $E_2 = E_3 = 7.2$ GPa, $G_{12} = G_{13} = G_{23} = 3.76$ GPa, $\nu_{12} = \nu_{13} = \nu_{23} = 0.29$ and $\rho = 1540$ kg/m^3.

Firstly, the assessment of the maximum transverse displacement is carried out for plates under uniformly distributed transverse load, i.e. $q(x, y) = q_0$, assuming six different boundary conditions: (i) fully simply supported (SSSS); (ii) fully clamped (CCCC); (iii) simply supported at $x = 0$ and a (SSFF); (iv) clamped at $x = 0$ and a (CCFF); (v) simply supported at $x = 0$ and $y = 0$ (SFSF) and (vi) clamped at $x = 0$ and $y = 0$ (CFCF). The maximum transverse displacements predicted by the UEL models are compared with those developed by Marques et al. [7], resorting to a FE model based on the FSDT. Even though Marques et al. [7] have only considered the case of thin plates ($a/h = 100$), the scenario of moderately thick plates ($a/h = 10$) is further investigated herein to thoroughly compare the UEL models for the various constrains. In addition, the nondimensionalized form given in Eq. (18) is adopted to present the predicted deflections concisely.

Furthermore, to provide a more insightful description and comparison of the UEL models predictive capabilities, particularly on the evaluation of the through-thickness distribution of displacements and stresses, the complete static analysis is carried out for moderately thick plates, with $a/h = 10$. It is assumed that the plates are simply supported and subjected to a bi-sinusoidally distributed transverse load as given in Eq. (17). Numerical results are also provided in the nondimensionalized form stated in Eq. (18).

As far as free vibration analysis is concerned, the natural frequencies associated to the first nine bending modes of each laminate are evaluated, considering both simply supported and clamped boundary conditions, as well as thin and moderately thick plates. Numerical results are compared with the benchmark solutions by Akhavan and Ribeiro [10], predicted by a FE model assigning the Reddy's TSDT. Additionally, considering the work by Viglietti et al. [18], the natural frequencies of the clamped *VSC1* and *VSC2*, predicted by a refined LW 1D CUF model, are included as well.

Although not shown, for both UEL models, a prior convergence analysis reveals that 30 × 30 elements ensure converged solutions for all laminates, side-to-thickness ratios and boundary conditions. Moreover, despite the various boundary conditions assumed throughout the numerical applications, the simply supported boundary conditions of the TSDT based model are exemplified as follows:

$$u_0^k = w_0^k = \theta_x^k = \varkappa_x^k = \lambda_x^k = 0 \quad \text{at } y = 0, a \tag{19a}$$

$$v_0^k = w_0^k = \theta_y^k = \varkappa_y^k = \lambda_y^k = 0 \quad \text{at } x = 0, a \tag{19b}$$

where $k = \{t, c, b\}$, noting that for the FSDT based model, the high-order generalized displacements ($\varkappa_x^k$, $\varkappa_y^k$, λ_x^k, λ_y^k) are not included.

Table 1
Static analysis results of the simply supported composite laminate (0/90/0), with $a/h = 100$ and 10, under bi-sinusoidal load: comparison with 3D exact solutions.

a/h	Model	$\tilde{u}\left(0, \frac{a}{2}, \frac{h}{2}\right)$	$\tilde{v}\left(\frac{a}{2}, 0, \frac{h}{2}\right)$	$\tilde{w}\left(\frac{a}{2}, \frac{a}{2}, 0\right)$	$\tilde{\sigma}_{xx}\left(\frac{a}{2}, \frac{a}{2}, \frac{h}{2}\right)$	$\tilde{\sigma}_{yy}\left(\frac{a}{2}, \frac{a}{2}, \frac{h}{2}\right)$	$\tilde{\sigma}_{xz}\left(0, \frac{a}{2}, 0\right)$
100	Exact [25]	−0.6780	−0.6823	0.4347	0.5393	0.0269	0.3947
	UEL1	−0.6778	−0.6822	0.4346	0.5398	0.0269	0.3940
	UEL3	−0.6780	−0.6823	0.4347	0.5394	0.0269	0.3950
10	Exact [25]	−0.7351	−1.0995	0.7530	0.5906	0.0429	0.3573
	UEL1	−0.7153	−1.0857	0.7402	0.5728	0.0399	0.3589
	UEL3	−0.7407	−1.1050	0.7556	0.5930	0.0426	0.3585

Table 2
First ten nondimensionalized natural frequencies $\tilde{\omega}_{mn} = \omega_{mn}\sqrt{\rho/E_0}(a^2/h)$ of the simply supported composite laminate (0/90/0), with $a/h = 10$: comparison with 3D exact solutions.

Model	$\tilde{\omega}_{11}$	$\tilde{\omega}_{12}$	$\tilde{\omega}_{01}$	$\tilde{\omega}_{10}$	$\tilde{\omega}_{21}$	$\tilde{\omega}_{13}$	$\tilde{\omega}_{22}$	$\tilde{\omega}_{23}$	$\tilde{\omega}_{02}$	$\tilde{\omega}_{20}$
Exact [25]	11.457	18.212	22.214	22.214	28.182	30.564	31.892	40.537	44.429	44.429
UEL1	11.568	18.379	22.215	22.215	28.653	30.979	32.366	41.159	44.429	44.429
UEL3	11.451	18.179	22.214	22.214	28.170	30.468	31.855	40.438	44.429	44.429

5.1. Analysis of CSC plates: Comparison with 3D exact solutions

The accuracy assessment of the UEL models is firstly presented considering a comparison with 3D exact static and free vibration solutions for simply supported multilayered plates with constant stiffness composite layers. Table 1 shows some static analysis results, considering both thin and moderately thick plates, with $a/h = 100$ and 10, respectively. All results are given at the absolute maximum in-plane location, alongside with the 3D exact solutions developed by Moleiro et al. [25].

Additionally, for the case of $a/h = 10$, Table 2 presents the first ten nondimensionalized natural frequencies predicted by the UEL models, as well as the associated 3D exact solutions in line with the previous benchmark work [25]. For each frequency, the in-plane mode shape (m, n), i.e. the number of half-waves in the x- and y-axis, respectively, is also indicated. It is underlined that the modes in the form of $(m, 0)$ and $(0, n)$, that emerge among the remaining bending modes, are special modes with null transverse displacement (i.e. purely extensional).

From the provided results, the following remarks can be pointed out:

- For thin plates, all static analysis results obtained by the UEL models are in excellent agreement with the 3D exact solutions. However, for moderately thick plates, the third-order model (UEL3) predicts displacements and stresses closer to the 3D exact solutions than the first-order model (UEL1);
- Although the transverse shear stresses are locally well predicted by both UEL models – even being derived from the constitutive equation – the UEL1 is not able to accurately describe the overall through-thickness distribution (as detailed in the following subsection).
- Both UEL models predict the first ten natural frequencies and mode shapes in fairly agreement with the 3D exact solutions, even thought the UEL3 is slightly more accurate when higher-order bending modes of moderately thick plates are of interest.

5.2. Static analysis of VSC plates

In view of the UEL models validation in static analysis of VSC laminates, Table 3 presents the (nondimensionalized) maximum transverse displacement of the four composite laminates, considering the case of both thin and moderately thick plates, with $a/h = 100$ and 10, respectively, subjected to uniform transverse load and various boundary conditions. For the case of thin plates, the results of the three VSC laminates are presented alongside with the solutions developed by Marques et al. [7] (FSDT). As expected due to high side-to-thickness ratio, the deflections predicted by both UEL models are in excellent agreement with the first-order ESL model [7], for all laminates and boundary conditions.

Table 3
Nondimensionalized maximum transverse displacement $\bar{w}_{\max}$ of laminated plates, with $a/h = 100$ and 10, under uniform transverse load and various boundary conditions.

Case	a/h	Model	SSSS	CCCC	SSFF	CCFF	SFSF	CFCF
CSC	100	UEL1	0.669	0.141	0.679	0.136	140.35	6.830
		UEL3	0.669	0.141	0.680	0.137	140.38	6.833
	10	UEL1	0.903	0.373	0.932	0.382	147.14	7.971
		UEL3	0.925	0.391	0.958	0.403	147.50	8.073
VSC1	100	FSDT [7]	0.553	0.210	1.019	0.288	59.997	7.584
		UEL1	0.549	0.210	1.019	0.286	59.402	7.580
		UEL3	0.550	0.210	1.020	0.286	59.507	7.585
	10	UEL1	0.785	0.455	1.506	0.627	65.765	9.290
		UEL3	0.809	0.474	1.546	0.654	66.668	9.421
VSC2	100	FSDT [7]	0.758	0.160	1.517	0.237	109.60	4.970
		UEL1	0.758	0.160	1.515	0.237	109.56	4.966
		UEL3	0.758	0.160	1.518	0.237	109.59	4.969
	10	UEL1	1.008	0.400	2.133	6.078	114.07	0.525
		UEL3	1.030	0.419	2.183	6.171	114.37	0.549
VSC3	100	FSDT [7]	0.682	0.141	13.266	1.357	72.674	6.572
		UEL1	0.675	0.141	13.268	1.352	70.938	6.570
		UEL3	0.675	0.141	13.271	1.353	70.987	6.572
	10	UEL1	0.925	0.373	13.777	1.774	76.916	7.616
		UEL3	0.948	0.391	13.840	1.807	77.504	7.705

However, for moderately thick plates, the results presented in Table 3 show that the FSDT based model (UEL1) underestimates the maximum transverse deflection compared to the TSDT based model (UEL3). In particular, the major discrepancy between the UEL1 and UEL3 models is found in the fully clamped plates, taking values slightly lower than 5%. Ultimately, a careful observation of Table 3 reveals that the CSC laminate outperforms the VSC laminates only for SSFF and CCFF boundary conditions.

To provide a more complete understanding and comparison of the UEL models accuracy in the assessment of all displacement and stress components, Table 4 presents the static analysis results of simply supported plates, with $a/h = 10$ (i.e. moderately thick), under bi-sinusoidal transverse load. All variables are shown using the nondimensionalized form given in Eq. (18). As apparent by the underlying results, from a practical standpoint, the solutions predicted by the UEL models are in good agreement with each other, except for the transverse shear stresses.

A more insightful description of the response behaviour of each laminate, predicted by each UEL model, is given in Figs. 3 to 6 (the interested reader is suggested to see the coloured version available online for a more easy and clear interpretation). Particularly, Fig. 3 illustrates the distribution of the transverse displacement along the x-axis at $y = a/2$, demonstrating that as one moves from the supports towards the centre, i.e. in the direction of the maximum deflection, the UEL3 model predicts successively higher transverse displacements

Table 4
Static analysis results of simply supported CSC and VSC laminates, with $a/h = 10$, under applied bi-sinusoidal transverse load.

Case	Model	$\tilde{u}\left(0, \frac{a}{2}, \frac{h}{2}\right)$	$\tilde{v}\left(\frac{a}{2}, 0, \frac{h}{2}\right)$	$\tilde{w}\left(\frac{a}{2}, \frac{a}{2}, 0\right)$	$\tilde{\sigma}_{xx}\left(\frac{a}{2}, \frac{a}{2}, \frac{h}{2}\right)$	$\tilde{\sigma}_{yy}\left(\frac{a}{2}, \frac{a}{2}, \frac{h}{2}\right)$	$\tilde{\sigma}_{xy}\left(0, 0, \frac{h}{2}\right)$	$\tilde{\sigma}_{xz}\left(0, \frac{a}{2}, 0\right)$	$\tilde{\sigma}_{yz}\left(\frac{a}{2}, 0, 0\right)$
CSC	UEL1	−0.671	−0.885	0.590	0.532	0.035	−0.026	0.379	0.082
	UEL3	−0.695	−0.908	0.605	0.551	0.036	−0.030	0.379	0.104
VSC1	UEL1	−0.489	−0.749	0.516	0.405	0.031	−0.930	0.291	0.029
	UEL3	−0.515	−0.777	0.532	0.427	0.032	−0.962	0.242	0.026
VSC2	UEL1	−0.737	−0.689	0.664	0.460	0.178	−0.053	0.327	0.127
	UEL3	−0.760	−0.713	0.679	0.479	0.185	−0.053	0.327	0.127
VSC3	UEL1	−0.514	−0.682	0.616	0.050	0.557	−0.967	0.094	0.456
	UEL3	−0.536	−0.705	0.631	0.051	0.577	−1.037	0.073	0.522

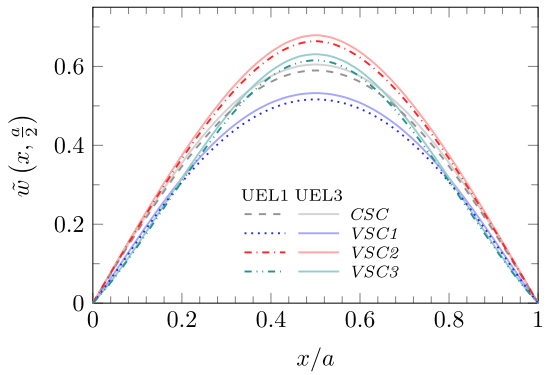

Fig. 3. Distribution of the nondimensionalized transverse displacement $\tilde{w}(x, a/2)$ along the x-axis of simply supported plates, with $a/h = 10$, under applied bi-sinusoidal load.

compared to the UEL1 model. However, according to Table 4, the maximum discrepancy between the models is around 3%, which indicates that they are in agreement with each other from a practical standpoint.

In addition, Fig. 4 shows the through-thickness distribution of the nondimensionalized in-plane displacements at the absolute maximum in-plane location. Likewise, Figs. 5 presents the through-thickness distribution of nondimensionalized in-plane normal stresses.

Finally, Fig. 6 presents the through-thickness profile of nondimensionalized transverse shear stresses derived from the constitutive equation, highlighting the major difference between the UEL models. In fact, the UEL1 model predicts a constant through-thickness distribution of transverse shear stresses in each layer, which has discontinuities in adjacent layers and violates the stress free boundary conditions on the upper and lower surfaces of the plate. On the other hand, the UEL3 model predicts a quadratic through-thickness distribution of transverse shear stresses, with vanishing transverse shear on the upper and lower surfaces of the plate, fulfilling approximately the interlaminar continuity conditions (even though not being imposed *a priori* in the formulation). Thus, comparing the numerical results shown in Table 4 and Fig. 6, one concludes that depending on the transverse coordinate, as well as on the laminate, the values predicted by the UEL models can be very similar or completely distinct. Although not shown, the discrepancy between the models on the evaluation of transverse shear stresses can be smoothed by the integration of the equilibrium equations, which imposes *a priori* the stress free boundary conditions, as well as the interlaminar continuity [24,26].

A close examination of Figs. 3 to 6 all together reveals several differences on the response behaviour of the four laminates. Even though only the *VSC1* reduces the maximum transverse displacement with respect to the *CSC* (Fig. 3), all VSC laminates have a lower maximum in-plane stress in the x-direction (Fig. 5) due to the variable fibre orientations. Furthermore, as shown by the numerical results shown in Table 4 and Fig. 5, the *VSC1* shows the lowest maximum in-plane stress in the y-direction as well.

Likewise, Fig. 6 shows that the distribution of transverse shear stresses σ_{xz} within the *VSC2* is analogous to *CSC*, but with an overall lower amplitude, which is solely outperformed – in the scene of lower stresses – by the *VSC3*. However, for the transverse shear stresses σ_{yz}, one concludes from Fig. 6 that the *VSC2* shows higher stress levels throughout the entire thickness when compared to the *CSC*, but lower than the *VSC3*.

Overall, among the numerical results presented in Table 4 and Figs. 3 to 6, the in-plane stresses and transverse shear stresses predicted by the higher-order model (UEL3) highlight for its slightly superior reliability, with respect to the first-order UEL1 model, when the emphasis of the analysis is to assess highly accurate descriptions at the layer level. Nevertheless, this discrepancy shall be more notorious as one considers lower side-to-thickness ratios, where the through-thickness distributions of displacements and stresses are more complex (i.e. non-linear).

5.3. Free vibration analysis of VSC plates

The assessment of the present models predictive capabilities in free vibration analysis of thin ($a/h = 100$) and moderately thick ($a/h = 10$) is shown in Tables 5 and 6, considering simply supported and clamped boundary conditions, respectively. In line with the benchmark solutions by Akhavan and Ribeiro [10], it is emphasized that only bending modes are evaluated. Thus, special modes with null transverse displacement, which emerge among the bending modes for the simply supported boundary conditions, are excluded.

For thin plates, either simply supported or clamped, the first nine natural frequencies predicted by the UEL models are in excellent agreement with those reported by Akhavan and Ribeiro [10]. However, for moderately thick plates, the discrepancy between the UEL3 model and the Reddy's TSDT model (ESL) [10] increases slightly. Actually, the advantages of refined LW descriptions shall be more pronounced as the side-to-thickness ratio decreases towards the case of thick plates.

Additionally, for both clamped *VSC1* and *VSC3*, the solutions developed by Viglietti et al. [18] (denoted by CUF) are included in Table 6 as an advanced structural model to further validate the UEL models with available benchmarks. As perceived from Table 6, both UEL models predict natural frequencies in fairly agreement with the CUF based model. In view of the presented UEL3 results for moderately thick plates, the highly accurate predictive capabilities of the high-order LW model in the free vibration analysis are shown through solutions closer to the LW 1D CUF based model by Viglietti et al. [18] than to the Reddy's TSDT model by Akhavan and Ribeiro [10] (throughout all nine modes of interest).

Moreover, for all laminates and side-to-thickness ratios, the UEL1 model predicts natural frequencies very close to the Reddy's TSDT model by Akhavan and Ribeiro [10]. Even though the discrepancy between the UEL1 model and the refined LW CUF model by Viglietti et al. [18] is higher, from a purely practical point of view, it is almost negligible. Therefore, comparing the UEL models, the UEL1 ensures a better compromise between accuracy and computational effort on the evaluation of the first natural frequencies of both thin and moderately thick VSC plates, either simply supported or clamped. Nevertheless, despite the increased computational cost of the higher-order LW model (UEL3), its piecewise cubic through-thickness distribution of in-plane

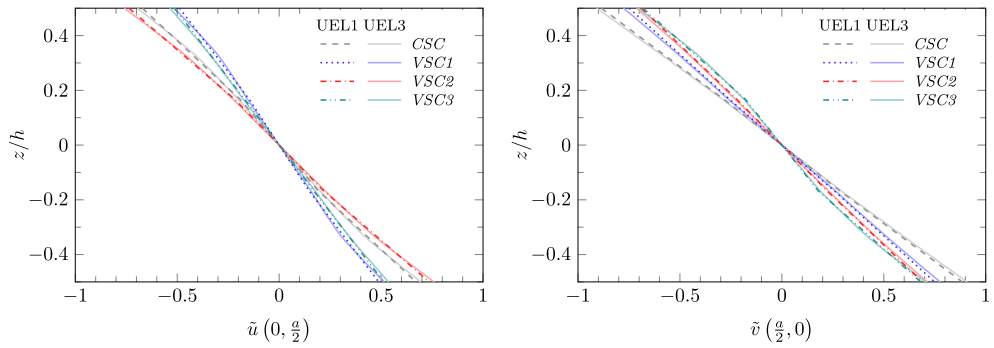

Fig. 4. Through-thickness distribution of nondimensionalized in-plane displacements $\tilde{u}$ and $\tilde{v}$ of simply supported plates, with $a/h = 10$, under applied bi-sinusoidal load.

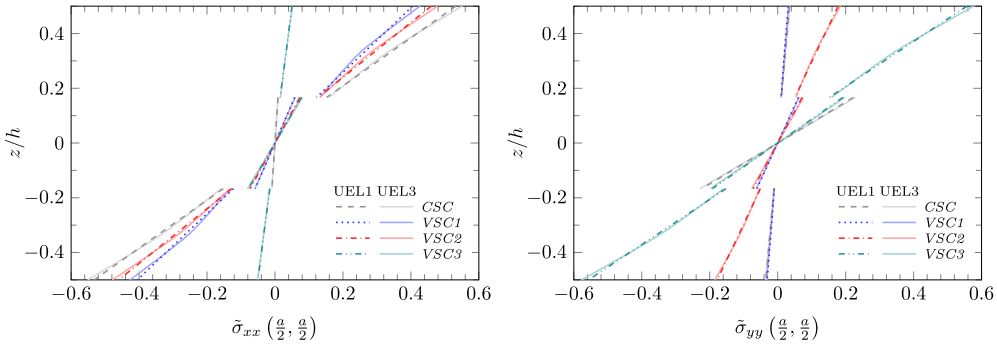

Fig. 5. Through-thickness distribution of nondimensionalized in-plane normal stresses $\tilde{\sigma}_{xx}$ and $\tilde{\sigma}_{yy}$ of simply supported plates, with $a/h = 10$, under applied bi-sinusoidal load.

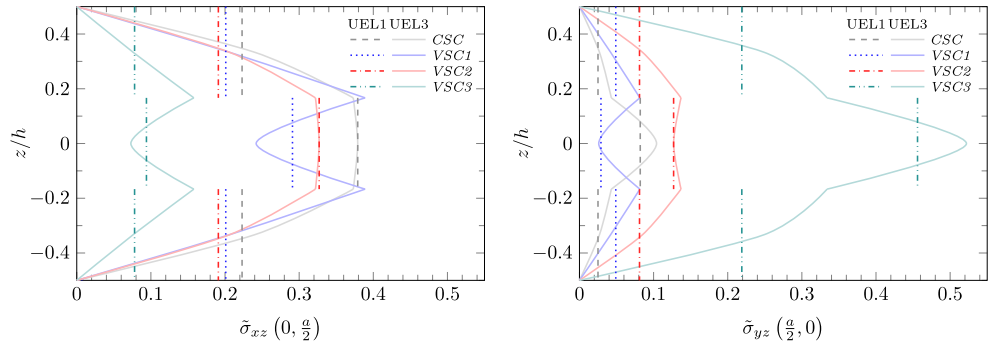

Fig. 6. Through-thickness distribution of nondimensionalized transverse shear stresses $\tilde{\sigma}_{xz}$ and $\tilde{\sigma}_{yz}$ of simply supported plates, with $a/h = 10$, under applied bi-sinusoidal load.

displacements is crucial for an accurate modelling of the behaviour of thick multilayered plates (as also shown by the prior comparison with 3D exact solutions for simply supported CSC plates).

A further remark may be noteworthy concerning the comparison of VSC laminates with respect to the CSC one, especially regarding the lowest natural frequencies and the mode shapes. For simply supported plates, the numerical results shown in Table 5 demonstrate that both *VSC1* and *VSC3* outperform the *CSC* in terms of the first three natural frequencies. On the other hand, for clamped plates, Table 6 reveals that only the *VSC3* has a fundamental frequency higher than the *CSC*. Additionally, as apparent in Fig. 7, the variable stiffness provides noticeable changes on the in-plane mode shapes in comparison to the case of the conventional straight fibre composites. Hence, a careful design of the fibre paths, as well as of the lamination scheme, should properly distribute the stiffness in such fashion that the desired mode shapes and natural frequencies can be achieved, at least in part.

6. Conclusions

In this work, user-elements in Abaqus are taken a step forward to render computationally efficient and numerically accurate static and free vibration analysis of VSC laminates, broadening the current state-of-the-art of refined multilayered UEL models and its available literature. The two LW user-element models, UEL1 and UEL3, are implemented using, for each discrete layer, the displacement field of the FSDT and TSDT, respectively. For the first time available, UEL models are purposely formulated to deal with the emerging and highly promising curvilinear fibre composites and a high-order LW description is implemented in the UEL subroutine, making progress on the high-order modelling of curvilinear fibre composites.

Numerical applications address a comprehensive assessment of the UEL models predictive capabilities in static and free vibration analysis of both CSC and VSC laminates. Firstly, the present models are validated by a comparison with 3D exact static and free vibration solutions for simply supported CSC plates. It is worth remarking that the obtained results are in agreement with the 3D exact solutions, for both thin and moderately thick plates, highlighting the successful implementation of the UEL models.

Furthermore, the models accuracy assessment in the analysis of VSC plates is presented for three laminates with linear fibre angle distributions. Various boundary and loading conditions are assumed, as well as

Table 5
First nine natural frequencies ω_n, in Hz, of thin and moderately thick plates, with $a/h = 100$ and 10, respectively, considering simply supported boundary conditions.

Case	a/h	Model	ω_1	ω_2	ω_3	ω_4	ω_5	ω_6	ω_7	ω_8	ω_9
CSC	100	UEL1	51.58	78.10	137.54	190.76	205.13	227.21	242.13	310.67	344.52
		UEL3	51.57	78.09	137.51	190.62	204.98	227.13	241.96	310.46	344.31
	10	UEL1	439.35	670.71	1112.04	1199.47	1318.10	1605.03	1671.43	2018.83	2046.06
		UEL3	433.90	663.71	1097.87	1167.70	1286.84	1571.71	1645.39	1955.15	2005.64
VSC1	100	TSDT [10]	57.06	93.89	152.85	171.12	211.34	234.70	274.81	340.13	360.06
		UEL1	56.78	93.56	152.57	170.80	210.42	232.97	273.22	330.56	354.29
		UEL3	56.74	93.49	152.46	170.66	210.21	232.81	272.92	330.28	353.86
	10	TSDT [10]	467.07	746.16	1114.23	1165.68	1348.32	1662.97	1735.90	1854.68	2039.23
		UEL1	468.66	746.23	1134.28	1164.10	1364.93	1658.07	1752.77	1890.28	2068.69
		UEL3	461.60	734.93	1107.02	1146.61	1333.52	1628.47	1713.78	1835.21	2011.24
VSC2	100	TSDT [10]	49.15	80.18	134.57	180.05	203.69	208.08	270.83	279.94	372.74
		UEL1	49.14	80.18	134.54	180.05	203.34	207.90	269.93	278.09	363.10
		UEL3	49.13	80.16	134.51	179.94	203.26	207.76	269.75	277.96	362.87
	10	TSDT [10]	417.05	672.55	1066.99	1133.38	1334.27	1482.87	1763.35	1871.98	1934.38
		UEL1	421.25	677.58	1074.66	1159.87	1358.07	1497.96	1778.07	1909.22	1959.67
		UEL3	416.49	670.58	1061.40	1130.81	1328.99	1474.46	1770.12	1858.77	1918.45
VSC3	100	TSDT [10]	52.47	85.85	141.07	173.67	203.70	223.11	279.40	288.04	352.78
		UEL1	52.26	85.33	140.26	172.75	201.63	221.02	269.91	283.34	343.63
		UEL3	52.24	85.30	140.21	172.63	201.49	220.89	265.76	283.17	343.33
	10	TSDT [10]	437.14	700.65	1100.69	1123.43	1313.72	1532.03	1775.99	1828.13	1969.63
		UEL1	439.74	703.97	1109.85	1146.25	1331.65	1549.74	1774.57	1858.29	2004.07
		UEL3	434.30	695.78	1095.57	1118.98	1304.24	1523.05	1744.65	1813.88	1952.67

Table 6
First nine natural frequencies ω_n, in Hz, of thin and moderately thick plates, with $a/h = 100$ and 10, respectively, considering clamped boundary conditions.

Case	a/h	Model	ω_1	ω_2	ω_3	ω_4	ω_5	ω_6	ω_7	ω_8	ω_9
CSC	100	UEL1	112.09	140.14	202.21	293.13	297.86	309.49	348.44	418.53	423.52
		UEL3	111.99	140.03	202.06	292.53	297.63	308.88	347.83	417.89	423.11
	10	UEL1	683.87	930.16	1332.24	1356.35	1486.65	1796.86	1891.07	2094.96	2201.59
		UEL3	667.54	912.15	1295.23	1331.49	1449.60	1756.61	1855.72	2034.31	2141.42
VSC1	100	TSDT [10]	92.21	130.75	195.09	237.74	274.85	282.52	339.92	388.90	430.80
		CUF [18]	92.90	132.28	198.97	240.46	278.75	291.12	346.60	404.07	444.97
		UEL1	92.25	130.76	195.06	237.92	275.02	282.42	339.84	388.42	430.39
		UEL3	92.18	130.67	194.92	237.54	274.59	282.18	339.33	388.02	429.77
	10	TSDT [10]	613.80	909.08	1232.39	1337.94	1484.89	1797.68	1931.29	1964.59	2151.17
		CUF [18]	609.79	903.63	1216.00	1328.41	1469.33	1774.84	1930.15	1931.36	2113.88
		UEL1	618.41	910.17	1238.78	1331.47	1489.51	1781.26	1933.09	1968.74	2149.38
		UEL3	605.49	893.80	1206.46	1307.55	1454.56	1745.29	1894.10	1912.88	2091.45
VSC2	100	TSDT [10]	106.18	137.34	196.50	270.73	282.59	302.79	361.25	367.76	458.30
		UEL1	106.22	137.36	196.51	270.88	282.69	302.90	361.06	367.33	456.57
		UEL3	106.14	137.26	196.36	270.53	282.29	302.39	360.50	366.93	455.91
	10	TSDT [10]	659.67	906.58	1299.78	1307.38	1521.87	1719.71	1944.31	2024.49	2156.96
		UEL1	663.53	908.69	1299.45	1303.73	1518.06	1715.21	1938.98	2001.37	2145.40
		UEL3	648.44	892.51	1268.38	1277.49	1483.23	1683.22	1901.90	1945.19	2104.18
VSC3	100	TSDT [10]	113.12	145.18	212.55	268.92	292.32	316.33	362.59	392.59	464.80
		CUF [18]	114.32	148.92	223.15	279.60	303.80	332.45	381.32	425.44	507.54
		UEL1	113.08	145.09	212.11	268.64	291.91	314.73	356.43	390.04	460.35
		UEL3	112.98	144.97	211.91	268.22	291.41	314.27	355.87	389.44	459.64
	10	TSDT [10]	681.85	917.02	1304.03	1312.60	1465.90	1714.09	1919.82	1990.01	2000.08
		CUF [18]	672.68	909.02	1270.07	1301.02	1441.95	1690.38	1904.58	1943.18	1943.44
		UEL1	686.34	920.18	1299.48	1312.40	1463.20	1706.61	1909.70	1968.58	1978.61
		UEL3	670.22	902.88	1263.80	1288.50	1430.05	1673.03	1874.52	1927.52	1949.01

the case of thin and moderately thick plates. As a result, the accuracy of the developed UEL models is demonstrated and discussed using different benchmarks available in the literature, such as ESL models (either FSDT or Reddy's TSDT) and refined LW 1D-CUF models. For the case of moderately thick plates, the UEL3 model improves the UEL1 on the evaluation of displacements, stresses and natural frequencies. However, even thought the piecewise cubic model (UEL3) demonstrates an overall advantage on characterizing the through-thickness response behaviour, the piecewise linear model (UEL1) ensures a better compromise between accuracy and computational effort, especially when thin plates are concerned.

Ultimately, the comparison of the different VSC laminates leads to the conclusion that through a careful design of the curvilinear fibre paths, one can ensure high global bending stiffness, tackling maximum deflections and natural frequencies, while locally tailoring the distribution of stresses and mode shapes. Therefore, refined structural models are crucial for an accurate analysis and design of VSC laminates. In effect, the two LW user-elements in Abaqus here proposed may allow further ensuing research, namely on design optimization of curvilinear fibre composites, analysis of variable stiffness sandwich panels, and even extension of UEL models to buckling and non-linear analysis.

CRediT authorship contribution statement

J.A. Moreira: Conceptualization, Methodology, Software, Validation, Formal analysis, Investigation, Resources, Data curation, Writing – original draft, Writing – review & editing, Visualization, Project administration, Funding acquisition. **F. Moleiro:** Conceptualization, Methodology, Writing – review & editing, Supervision, Project administration, Funding acquisition. **A.L. Araújo:** Conceptualization, Methodology, Writing – review & editing, Supervision, Funding acquisition.

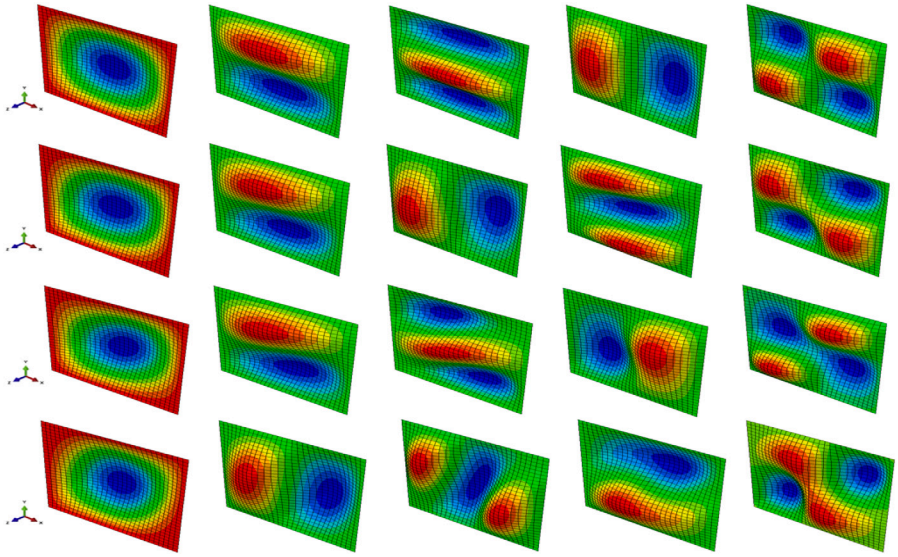

Fig. 7. First five in-plane bending mode shapes $w(x, y, 0)$ of the simply supported *CSC* (1st line), *VSC1* (2nd line), *VSC2* (3rd line) and *VSC3* (4th line), with $a/h = 10$, predicted by the UEL3.

A. Pagani: Conceptualization, Writing – review & editing, Supervision, Funding acquisition.

Declaration of competing interest

The authors declare that they have no known competing financial interests or personal relationships that could have appeared to influence the work reported in this paper.

Data availability

Data will be made available on request.

Acknowledgments

This work has been supported by National Funds through Fundação para a Ciência e Tecnologia (FCT), through IDMEC, under LAETA, project UIDB/50022/2020. The first author (J.A. Moreira) appreciates the financial support of FCT through the PhD Grant 2021.06113.BD. In addition, A. Pagani acknowledges funding from the European Research Council (ERC) under the European Union's Horizon 2020 research and innovation programme (Grant agreement No. 850437).

References

[1] Kim BC, Potter K, Weaver PM. Computer aided modelling of variable angle tow composites manufactured by continuous tow shearing. Compos Struct 2015;129:256–67. http://dx.doi.org/10.1016/j.compstruct.2015.04.012.

[2] Oromiehie E, Prusty BG, Compston P, Rajan G. Automated fibre placement based composite structures: Review on the defects, impacts and inspections techniques. Compos Struct 2019;224:110987. http://dx.doi.org/10.1016/j.compstruct.2019.110987.

[3] Gurdal Z, Olmedo R. In-plane response of laminates with spatially varying fiber orientations - Variable stiffness concept. AIAA J 1993;31(4):751–8. http://dx.doi.org/10.2514/3.11613.

[4] Olmedo R, Gurdal Z. Buckling response of laminates with spatially varying fiber orientations. In: 34th structures, structural dynamics and materials conference. la Jolla, California, USA: AIAA; 1993, https://arc.aiaa.org/doi/abs/10.2514/6.1993-1567.

[5] Abdalla MM, Setoodeh S, Gurdal Z. Design of variable stiffness composite panels for maximum fundamental frequency using lamination parameters. Compos Struct 2007;81(2):283–91. http://dx.doi.org/10.1016/j.compstruct.2006.08.018.

[6] Lopes CS, Gurdal Z, Camanho PP. Tailoring for strength of composite steered-fibre panels with cutouts. Composites A 2010;41(12):1760–7. http://dx.doi.org/10.1016/j.compositesa.2010.08.011.

[7] Marques FEC, da Mota AFS, Loja MAR. Variable stiffness composites: Optimal design studies. J Compos Sci 2020;4(2). http://dx.doi.org/10.3390/jcs4020080.

[8] Stodieck O, Cooper JE, Weaver PM, Kealy P. Improved aeroelastic tailoring using tow-steered composites. Compos Struct 2013;106:703–15. http://dx.doi.org/10.1016/j.compstruct.2013.07.023.

[9] Guimarães TAM, Castro SGP, Cesnik CES, Rade DA. Supersonic flutter and buckling optimization of tow-steered composite plates. AIAA J 2019;57(1):397–407. http://dx.doi.org/10.2514/1.J057282.

[10] Akhavan H, Ribeiro P. Natural modes of vibration of variable stiffness composite laminates with curvilinear fibers. Compos Struct 2011;93(11):3040–7. http://dx.doi.org/10.1016/j.compstruct.2011.04.027.

[11] Akhavan H, Ribeiro P, de Moura MFSF. Large deflection and stresses in variable stiffness composite laminates with curvilinear fibres. Int J Mech Sci 2013;73:14–26. http://dx.doi.org/10.1016/j.ijmecsci.2013.03.013.

[12] Yazdani S, Ribeiro P, Rodrigues JD. A p-version layerwise model for large deflection of composite plates with curvilinear fibres. Compos Struct 2014;108:181–90. http://dx.doi.org/10.1016/j.compstruct.2013.09.014.

[13] Yazdani S, Ribeiro P. Geometrically non-linear static analysis of unsymmetric composite plates with curvilinear fibres: p-version layerwise approach. Compos Struct 2014;118:74–85. http://dx.doi.org/10.1016/j.compstruct.2014.07.007.

[14] Yazdani S, Ribeiro P. A layerwise p-version finite element formulation for free vibration analysis of thick composite laminates with curvilinear fibres. Compos Struct 2015;120:531–42. http://dx.doi.org/10.1016/j.compstruct.2014.10.030.

[15] Demasi L, Biagini G, Vannucci F, Santarpia E, Cavallaro R. Equivalent single layer, zig-zag, and layer wise theories for variable angle tow composites based on the generalized unified formulation. Compos Struct 2017;177:54–79. http://dx.doi.org/10.1016/j.compstruct.2017.06.033.

[16] Tornabene F, Fantuzzi N, Bacciocchi M. Higher-order structural theories for the static analysis of doubly-curved laminated composite panels reinforced by curvilinear fibers. Thin-Walled Struct 2016;102:222–45. http://dx.doi.org/10.1016/j.tws.2016.01.029.

[17] Sánchez-Majano AR, Azzara R, Pagani A, Carrera E. Accurate stress analysis of variable angle tow shells by high-order equivalent-single-layer and layer-wise finite element models. Materials 2021;14(21). http://dx.doi.org/10.3390/ma14112706.

[18] Viglietti A, Zappino E, Carrera E. Analysis of variable angle tow composites structures using variable kinematic models. Composites B 2019;171:272–83. http://dx.doi.org/10.1016/j.compositesb.2019.03.072.

[19] Viglietti A, Zappino E, Carrera E. Free vibration analysis of variable angle-tow composite wing structures. Aerosp Sci Technol 2019;92:114–25. http://dx.doi.org/10.1016/j.ast.2019.05.068.

[20] Yan Y, Liu B, Xing Y, Carrera E, Pagani A. Free vibration analysis of variable stiffness composite laminated beams and plates by novel hierarchical differential quadrature finite elements. Compos Struct 2021;274:114364. http://dx.doi.org/10.1016/j.compstruct.2021.114364.

[21] Pagani A, Sánchez-Majano AR. Influence of fiber misalignments on buckling performance of variable stiffness composites using layerwise models and random fields. Mech Adv Mater Struct 2020;1–16. http://dx.doi.org/10.1080/15376494.2020.1771485.

[22] Pagani A, Sánchez-Majano AR. Stochastic stress analysis and failure onset of variable angle tow laminates affected by spatial fibre variations. Composites C 2021;4:100091. http://dx.doi.org/10.1016/j.jcomc.2020.100091.

[23] Ferreira GFO, Almeida Jr JHS, Ribeiro ML, Ferreira AJM, Tita V. Development of a finite element via unified formulation: Implementation as a user element subroutine to predict stress profiles in composite plates. Thin-Walled Struct 2020;157:107107. http://dx.doi.org/10.1016/j.tws.2020.107107.

[24] Moreira JA, Moleiro F, Araújo AL. Layerwise electro-elastic user-elements in abaqus for static and free vibration analysis of piezoelectric composite plates. Mech Adv Mater Struct 2022;29(21):3109–21. http://dx.doi.org/10.1080/15376494.2021.1886381.

[25] Moleiro F, Mota Soares CM, Carrera E, Reddy JN. Evaluation of exact electro-elastic static and free vibration solutions of multilayered plates for benchmarking: piezoelectric composite laminates and soft core sandwich plates. Composites C 2020;2. http://dx.doi.org/10.1016/j.jcomc.2020.100038.

[26] Reddy JN. Mechanics of laminated composite plates and shells – theory and analysis. 2nd ed.. Boca Raton: CRC Press; 2004.

[27] Birman V, Bert CW. On the choice of shear correction factor in sandwich structures. J Sandw Struct Mater 2002;4:83–95. http://dx.doi.org/10.1177/1099636202004001180.

[28] Pagano NJ. Exact solutions for rectangular bidirectional composites and sandwich plates. J Compos Mater 1970;4:20–34. http://dx.doi.org/10.1177/002199837000400102.